Rapid radon potential classification using soil-gas radon measurements in the Cooley Peninsula (County Louth, Ireland)

Elío J.[(1)], Crowley Q.[(1)], Scanlon R.[(2)], Hodgson J.[(2)], Long S.[(3)]

(1) Geology, School of Natural Sciences, Trinity College, Dublin 2, Ireland

(2) Geological Survey, Ireland

(3) Environmental Protection Agency of Ireland, Ireland

Corresponding author: Elío J.

Email: elioj@tcd.ie – javiereliomedina@gmail.com

Postal address: Museum Building, Geology, School of Natural Sciences, Trinity College, Dublin 2, Ireland

Abstract

A rapid method for local-scale radon risk assessment using in-situ radon soil-gas measurements and a national-scale soil permeability dataset have been evaluated. We test and validate our approach in a case study at the Cooley Peninsula (County Louth, Ireland). In total 60 radon soil-gas measurements from 48 points were carried out in an area of approximately 160 km^2 over a five day period. Results of radon potential classification are compared with the legislative indoor radon map of Ireland, with more than 400 indoor radon measurements in the study area.

Soil-gas radon concentrations in the Cooley Peninsula ranged from very low values (< 10 kBq m^{-3}) to extremely high (up to 112 kBq m^{-3}), whereas indoor radon concentrations ranged from 3 to 863 Bq m^{-3}. The Cooley Peninsula is therefore mostly classified as a Moderate-High and High radon potential area. The percentage of indoor radon variance explained by soil-gas radon concentration, soil permeability and geology is approximately 30% (12%, 9.3% and 8.6%; respectively).

Our findings show that radon potential classification can detect radon priority areas with a reasonable degree of accuracy, even with a relatively low number of point measurements in relation to the size of the area studied. We demonstrate that active radon measurements and geostatistical modelling can significantly reduce the time and cost required to evaluate an area in relation to expected indoor radon concentrations. This approach is viable to produce a radon potential map in rural areas, or

where land-use has been re-designated for new housing, where few or no indoor radon measurements are available.

Keywords: Radon, geogenic radon map, radon potential, soil-gas, indoor radon

1. Introduction

Radon exposure is the highest source of natural ionizing radiation to the global population (UNSCEAR 2000), representing a significant radiological hazard with measurable detrimental health effects. The World Health Organisation (WHO) classified radon as a Class 1 carcinogen and it is estimated that radon is the second cause of lung cancer after smoking (e.g. Field, 2015; US-EPA, 2003; WHO, 2010). In Europe, for example, approximately 10% of lung cancers are linked to radon (McColl et al. 2015).

Radon is a radioactive gas which forms as a decay product of radium (Ra) generated in the radioactive decay series of uranium (U) and thorium (Th). The three natural isotopes are radon (^{222}Rn), thoron (^{220}Rn) and actinon (^{219}Rn), which come from the decay series of ^{238}U, ^{232}Th and ^{235}U, respectively (Cothern and Smith 1987). However, due to the half-life of radon ($T_{1/2}$ = 3.82 d) relative to the short half-life of thoron ($T_{1/2}$ = 55.6 s) and actinon ($T_{1/2}$ = 3.96 s) the radon risk in indoor air is principally caused by the ^{222}Rn isotope (Adepelumi et al. 2005; Oufni et al. 2013). The progeny can be attached to aerosols (i.e. suspended particles, water droplets) and inhaled. Progeny daughter isotopes may deposit in the respiratory track, where the alpha radiation interacts with lung tissue leading to DNA damage and development of lung cancer (Cothern and Smith 1987; WHO 2009).

The decay series of ^{238}U is:

$$^{238}\text{U}\ (4.5\text{Ga}) \xrightarrow{\alpha} {}^{234}\text{Th}\ (24\text{d}) \xrightarrow{\beta} {}^{234}\text{Pa}\ (1.2\text{min}) \xrightarrow{\beta} {}^{234}\text{U}\ (0.25\text{Ma}) \xrightarrow{\alpha} {}^{230}\text{Th}\ (75\text{Ka}) \xrightarrow{\alpha} {}^{226}\text{Ra}\ (1.6\text{Ka}) \xrightarrow{\alpha}$$
$$^{222}\text{Rn}\ (3.8\text{d}) \xrightarrow{\alpha} {}^{218}\text{Po}\ (3.1\text{min}) \xrightarrow{\alpha} {}^{214}\text{Po}\ (26.8\text{min}) \xrightarrow{\beta} {}^{214}\text{Bi}\ (19.9\text{min}) \xrightarrow{\beta} {}^{214}\text{Po}\ (164\mu\text{s}) \xrightarrow{\alpha} {}^{210}\text{Pb}$$
$$(22.3\text{a}) \xrightarrow{\beta} {}^{210}\text{Bi}\ (5\text{d}) \xrightarrow{\beta} {}^{210}\text{Po}\ (138\text{d}) \xrightarrow{\alpha} {}^{206}\text{Pb}\ (\text{stable})$$

All elements of the series are solid except ^{222}Rn. Thus, their mobility are limited and are principally produced by dissolution or particulate adsorption processes in aqueous media. Radon gas, however, escapes from minerals in soils and rocks and is found both in groundwater and soil gas (Bonotto and Andrews 1999). When radon reaches the atmosphere, it is easily diluted so its outdoor concentration is normally low, in the order of 5-10 Bq m^{-3} (e.g. Appleton et al., 2011a; Dubois, 2005; Gunning et al.,

2014; Scheib et al., 2013); however, within dwellings and other confined places (e.g. workplaces, caves) radon may be trapped and accumulate to reach high concentrations.

Indoor radon principally comes from the surrounding soils on which they are located (e.g. Adepelumi et al. 2005), although it may also originate from building materials (Azam et al. 1995; Capaccioni et al. 2012) and groundwater used in the building (Cothern 1999; UNSCEAR 2006). In the soil, radon has three principal origins and it may be: i) generated in the soil by the presence of ^{226}Ra (e.g. Greeman and Rose, 1996; Tanner, 1978); ii) released from groundwater, both because it is transported by groundwater or it is generated in it (e.g. Guerra and Etiope, 1999; Porcelli, 2008; Schubert et al., 2001); and iii) carried by other gases with a deeper origin, i.e. CO_2 or CH_4 (e.g Elío et al., 2015; Etiope and Martinelli, 2002; Giammanco et al., 2009, 2007).

Radon enters into buildings by diffusive and advective processes (Andersen 2001), however due to its short half-life (i.e. $t_{1/2}$ = 3.8 days) advective processes are the main factor controlling the presence of radon indoors. Radon mobility by diffusion depends on its diffusivity and half-life (i.e. $L = \sqrt{D/\lambda}$, $C_x = C_0 e^{-(x/L)}$; where L is the diffusion length, D is the diffusion coefficient [10^{-9} m^2 s^{-1} in water and $1.2 \cdot 10^{-5}$ m^2 s^{-1} in air], λ is the decay constant, and C_x and C_0 are the ^{222}Rn concentration at a distant X and 0 from its source respectively; Bonotto and Andrews 1999; Huxol et al. 2012). The diffusion length of radon is therefore 2.4 metres in air and 2.2×10^{-2} metres in water. This means that in static conditions only about 1% (X = 5L) of the initial radon reaches a distance of 12 metres in air, and 0.15 metres in water. In soils the effective diffusion coefficient depends on the water saturation and soil porosity (Prasad et al. 2012) and may vary by some orders of magnitude; e.g. from $3 \cdot 10^{-6}$ m^2 s^{-1} in sand, $8 \cdot 10^{-9}$ m^2 s^{-1} in argillite, or $2 \cdot 10^{-9}$ m^2 s^{-1} in concrete (Cothern and Smith 1987), which makes diffusive transport only effective at a scale of a few metres. Longer migration distances require advective forces such as a dissolved phase in water, or transport together with other gas phases.

Indoor radon concentration depends therefore on soil properties (i.e. U-Ra concentration, radon concentration in the soil, permeability, temperature, water saturation; e.g. Appleton and Miles, 2010; Scheib et al., 2013), meteorological parameters (i.e. temperature, barometric pressure, humidity, indoor-outdoor pressure differences; e.g. Andersen, 2001; Groves-Kirkby et al., 2015), building characteristics (i.e. building material, preventive measures, ventilation; e.g. Capaccioni et al., 2012; Chen et al., 2010; Long et al., 2013), and other variables which are more difficult to quantify (Gunby et al. 1993). Understanding these processes is fundamental to radon risk assessment.

1.1. Radon mapping

Current indoor radon monitoring strategies generally use passive radon measurement to predict the probability of a dwelling having an indoor radon concentration above a reference level (e.g. Hodgson and Carey, 2013), with geological information included in order to forecast radon priority areas (e.g. Bossew, 2015; Ferreira et al., 2016; Pásztor et al., 2016). This dual approach of using both indoor radon concentration and geological information is the basis of the European strategy used to develop both the European Indoor Radon Map (EIRM) and the European Geogenic Radon Map (EGRM) (Tollefsen et al. 2014; Bossew et al. 2015). Radon maps are useful to inform government policy on building regulations in relation to radon as a natural hazard. Additionally, they can also be used to ensure that preventive measures and awareness campaigns are more accurately targeted to high risk areas.

The principal cause of error in indoor radon maps is that the spatial autocorrelation of observations is not analysed; for example, it is common to divide an area into grids (e.g. 10 x 10 km) and estimate the probability of radon concentrations above a reference level for each grid (Tollefsen et al. 2014). Therefore, while surveys of indoor radon have been instrumental in raising public awareness of radon, the resultant hazard maps may be limited by an uneven distribution of tested homes or sites, uncertainties in the exact locations of tested homes and extensive areas with little or no testing. As such, these maps are a good starting point to highlight some high radon areas, but they may be of limited use in a high-resolution predictive capacity (Appleton et al., 2011c). On the other hand, geogenic radon hazard maps have effectively demonstrated the complexity required to obtain reliable maps at a national scale (Bossew et al. 2015). It is worth noting however, that neighbouring houses may have very different indoor radon concentration (US-EPA 2001), indicating that factors in addition to geogenic attributes, (e.g. building, environment; Sarra et al., 2016) affect indoor radon concentration and spatial distribution.

Radon exposure poses a significant radiological hazard in Ireland, as it represents over 56% of the total radiation dose received by the Irish population (Colgan et al. 2008). Ireland has been classified as one of the countries with the highest levels of radon in Europe and eighth highest average of an OECD survey of 29 countries (Long et al. 2013). In fact, it was estimated that over 280 case of lung cancer in Ireland (approx. 12%) are directly linked to radon exposure every year (Elío et al. 2018). In Ireland, after introduction of national building regulations in 1998, it was reported that the average indoor radon concentration was reduced from 89 Bq m^{-3} to 77 Bq m^{-3} (Dowdall et al. 2017). The Irish building regulations state that new houses in a High Risk Area must have a radon preventive measure. The

current radon monitoring strategy in Ireland uses passive indoor radon measurement (Hodgson and Carey 2013) to define areas of high radon risk. The present study was designed to better understand the origin of radon in the natural environment and, therefore, to try to rapidly detect radon priority areas at a local scale, with a greater degree of spatial accuracy and without the necessity of using indoor measurements.

The large number of available indoor radon data in Ireland, with more than 30,000 dwellings sampled and geo-reference nationwide (Hodgson et al., 2014), represent an invaluable opportunity to analyse the relationship between indoor radon concentration and geogenic factors. In this regard, soil-gas radon concentration was measured in a case study in the Cooley Peninsula (County Louth, Ireland), which has approximately 400 indoor radon measurements. These indoor data are used as a means to validate our designation of radon priority areas based on radon soil-gas concentrations and a national subsoil permeability map. The conclusion obtained in this research may have application in other countries with similar meteorological conditions and building construction standards.

2. Material and methods

2.1. Study area

The methodology for site classification proposed in this study was tested in the Cooley Peninsula (County Louth), located in the North-East of the Republic of Ireland (Figure 1). This zone has been classified as a High Radon Risk Area by the Environmental Protection Agency of Ireland, based on indoor radon measurements (Fennell et al. 2002). The sample area is approximately 160 km^2, is underlain by several different geological units, in terms of chronostratigraphy (Silurian, Carboniferous, Tertiary), rock types (igneous, sedimentary and metamorphic) and surficial deposits (the geological map with a complete legend can be viewed in the GSI Spatial Resources Viewer portal; www.gsi.ie).

The Cooley Peninsula forms part of the Carlingford Complex, which started to form around 61 Ma (Baxter 2008). The bedrock geology is dominated by igneous rock types, with the presence of basalt (Tertiary minor volcanics Formation), gabbro (Tertiary basic intrusion Formation) and granite (Tertiary granite, felsite Formation) in the centre of the Cooley Peninsula (Figure 1). The south-eastern part is dominated by Carboniferous limestone (Marine shelf facies Formation) and the northern and south-western by Silurian metasediments (Silurian sandstone, greywacke, shale Formation) (Figure 1). The area was highly influenced by glaciations (Baxter 2008), resulting in glacial tills as a predominant

171 Quaternary sediment. Peaty topsoils also occur overlying bedrock in the centre part of the peninsula
172 (Gallagher et al. 2016). The direction of the main faults is NW-SE (GSI geological map of Ireland).
173
174 **2.2. Soil-gas radon measurements**
175
176 Forty eight locations were sampled in the Cooley Peninsula from 25th to 29th July 2016 (Figure 1), with
177 60 radon measurement carried out in total. One site (site nine) was used as a "control point", where
178 soil-gas radon was measured six times over the five days of field work, in order to check for possible
179 variation of radon levels due to changes in atmospheric conditions. Seven random field replicates were
180 measured in order to analyse the reproducibility of soil-gas radon measurements (points 2, 14, 25, 29,
181 30, 32, 33). The replicates were carried out by repeating the measurement procedure over a few
182 minutes and in a second site separated by approximately 1 meter.
183
184 Radon concentration in the soil-gas was measured with a pulse ionization chamber detector RM-2
185 (Elío et al., 2015). The soil-gas sampling was carried out with a hollow probe inserted into the ground
186 at 75–100 cm depth, in order to minimize the influence of atmospheric factors (Schubert and Schulz
187 2002; Schubert et al. 2005; García-González et al. 2008). Prior to taking the soil-gas sample the probe
188 was purged to avoid air contamination. The humidity and particulate material were removed by a
189 Drierite desiccant (anhydrous calcium sulphate) and a particle filter (0.45 µm), respectively. The first
190 two soil-gas samples were discarded and the third sample (150 mL) was introduced into a pre-
191 evacuated ionization chamber (250 mL). Finally, external air (with a negligible radon concentration
192 relative to soil-gas; i.e. 5 - 10 Bq m^{-3}) was introduced into the chamber to equalize the pressure in the
193 chamber to atmospheric pressure. The detection limit of the RM-2 device is 3 kBq m^{-3}, while the
194 uncertainty of radon concentration (1σ) is $0.33 \cdot (C_{Rn})^{0.5}$, where C_{Rn} is the concentration of radon ($C_{Rn} \pm$
195 σ). Thus, the uncertainty of radon measurement using the RM-2 instrument is below 20%.
196 Geostatistical analysis was carried out to predict a soil-gas radon value over a grid of 100 x 100 m.
197
198 **2.3. Subsoil permeability**
199
200 Subsoil permeability was obtained from the national Groundwater Recharge Map of Ireland
201 (downloaded from www.gsi.ie). The Geological Survey Ireland (GSI) classified the subsoil permeability
202 as "High", "Moderate" or "Low", based on direct measurements, observation of drainage patterns and
203 vegetation, particle size analysis as a permeability predictor, and subsoil descriptions using the British
204 Standard (BS)5930 (BSI 1999) as a proxy for particle size analysis (Hunter Williams et al. 2013). Where
205 subsoil was less than 3m thick (Depth to Bedrock; DTB, <3m), the GSI did not classify subsoil

permeability as it can be very spatially variable due to rooting, cracking and the influence of underlying bedrock (Lee et al. 2008; Masterson et al. 2008).

2.4. Radon risk classification and mapping

Sites were classified based on the "radon potential" index (Neznal et al. 2004), which takes into account the soil-gas radon concentration and the permeability of the soil. Radon potential (RP) is estimated as follows:

$$RP = \frac{C_{Rn}}{(-log_{10}(k) - 10)}$$

Where C_{Rn} is the equilibrium radon concentration in soil-gas (kBq m^{-3}) and k the soil permeability (m^2). The values of radon and permeability used in the RP formula were assigned values according to a categorization of each parameter (Table 1). In areas where the subsoil was less than 3 m thick (Depth to Bedrock, DTB, <3 m; total area: 59 km^2) the worst case scenario for radon risk assessment was assumed, and a high permeability value was assigned for the radon potential estimation.

With the combination of soil-gas radon predictions (grids of 100 x 100 m) and permeability values, a radon potential map was generated. The initial values obtained at 100 x 100 m were then aggregated to grids of 1 x 1 km, applying a weighted arithmetic mean of the different RP in each grid ($RP = \frac{1}{A_T}\sum_{i=1}^{n} A_i \cdot RP_i$ and $A_T = \sum_{i=1}^{n} A_i$; where RP and AT are the radon potential and the total area of a specific grid, respectively; and RP_i and A_i the radon potential and the area of the different subdivisions present in the grid, respectively). An area may be classified as: i) low risk (RP < 10), moderate-low risk (10 <= RP < 22.5), moderate-high risk (22.5 <= RP < 35) and high risk (RP > 35) (Figure 2).

2.5. Indoor Radon Measurements

Indoor radon measurements (n = 429) were used to validate the radon risk designations (Figure 1). Indoor radon concentration measurements (Figure 1) were carried out by the Environmental Protection Agency of Ireland (EPA), as part of a national survey in Irish dwellings between 1992 and 1999 (Fennell et al. 2002), and geo-referenced by the Geological Survey, Ireland (Hodgson et al. 2014) and Ireland's Health Services (HSE-Health Intelligence Unit; HSE, 2013). Indoor radon was sampled using passive alpha track detectors (CR-39), which were located in homes for a minimum of 3 months and seasonally adjusted to give an annual value (Burke et al. 2010). Finally, the annual values were

corrected by subtracting the average outdoor radon concentration of Ireland which improves the log-normal distribution of the data (i.e. 5.6 Bq m^{-3}; Gunning et al., 2014; Hodgson et al., 2014).

Ireland follows the recommendations of the European Commission (EURATOM 2013) and has adopted a national reference level for domestic indoor radon concentration of 200 Bq m^{-3} (NRCS 2014). A radon risk map was developed solely using indoor radon measurements (Fennell et al. 2002; www.radon.ie). The probability of having an indoor radon concentration above the reference level was estimated by grids of 10 x 10 km, and then the country was divided in five percentage bands; i.e., <1%, 1-5%, 5-10%, 10-20% and >20%. A "High Risk Area" was defined when the probability is 10% or higher. The study area of the Cooley Peninsula is one of such area.

3. Results

3.1. Soil-gas radon concentration

Soil-gas radon concentrations ranged between 3.5 kBq m^{-3} (# 46) and 112 kBq m^{-3} (# 28) (Table 2). According to the classification of radon concentration in soil-gas (Table 1), 3 points had very low concentrations (approx. 6%; points 12, 26 and 46), 12 had low concentrations (25%; points 1, 3, 11, 13, 17, 20, 24, 25, 29, 33 and 43), 20 moderate (42%; points 4-6, 9, 10, 16, 18, 19, 22, 23, 31, 32, 35-40, 42 and 48), 7 high (15%; points 2, 7, 14, 21, 30, 41 and 47), 5 very high (10%; points 8, 27, 34, 44 and 45), and 1 extremely high (2%; point 28). The Box-Cox transformation illustrate that the data do not follow either a normal nor log-normal distribution, and the optimal transformation is with a lambda of 0.50 (Figure 3a, b, and c) which was used for the data analysis. The data for control points and replicas were given in Table 3, the Relative Standard Deviation (RSD [%]) in the control point was 10% (point 9), while in the replicas (points 2, 14, 25, 29, 30, 32, 33; Table 3), the RSD was normally below 25%, except for point 32 in which the RSD was 50%.

The Relative Standard Deviation (RSD [%]) in the control point (i.e. 10%) and in the replicates (normally below 25%) are in accordance with the uncertainty of the instrument, less than 20%. The slight increase in uncertainty may be related to the higher variations under non-controlled conditions (i.e. fieldwork). Furthermore, the values obtained for the control point do not follow any trend (increase or decrease during the week), with the highest values in the second day (44.5 kBq m^{-3}) and the lowest the first day (33.3 kBq m^{-3}), suggesting that radon was not significantly affected by external parameters (i.e atmospheric conditions) during fieldwork, and the soil-gas radon measurements are deemed

suitable for further data analysis. In the points where more than one value is available (i.e. replicas and control point), the mean value of the measurements were assigned as the value of the point. In the anomaly point (#32) a mean value was also assigned as there are no criteria to select one of them (55.8, 26.7 or the mean 41.3 kBq m^{-3}).

Geostatistic analysis shows that the experimental variogram (point) was within the envelope (dotted lines) of all variograms obtained by random permutations of the data (Figure 3d). Thus it might be considered as the product of a random process with no spatial relationship existing between data points. The interpolation should be carried out therefore by non-geostatical methods; i.e. inverse distance weighted (Bivand et al. 2008). In our case, the interpolation was carried out with an inverse distance weighting power of 2 and a maximum number of nearest points (nmax) of 10 (Figure 4a).

3.2. Radon potential (RP)

A radon potential map was developed taking into account the estimated soil-gas radon concentrations (Figure 4a) and subsoil permeability in the Cooley Peninsula (Figure 4b). The resulting radon potential map (grids of 1 x 1 km) is shown in Figure 5. RP correspond principally with High (H) and Moderate-High (M-H) classification, and a very small percentage to Low (L) associated with the lowest values of radon concentration in soil-gas (points 12, 26 and 46; Figure 1 and Table 2). The percentage of M-H and H grids is 43% and 41%, respectively. This high radon potential classification is in agreement with the EPA results which classified the Cooley Peninsula as a High Radon Risk Area (areas where the probability of having an indoor radon concentration higher than the reference level of 200 Bq m^{-3} is 10% or higher, Figure 6).

3.3. Indoor radon measurements

Indoor radon concentration in the study area follow a lognormal distribution (n = 429). Indoor radon ranged between 2.4 and 863 Bq m^{-3} with a median of 46.5 Bq m^{-3}, a geometric mean of 49.54, and a geometric standard deviation of 2.83. From the 429 dwellings sampled in the area, 42 (9.8%) had indoor radon concentration above the reference level of 200 Bq m^{-3} (red stars in Figure 6). From the six 10 x 10 km grids sampled, 3 are grids where the EPA estimated a percentage of dwellings above the reference level higher than 20%, 2 between 10% and 20%, and 1 between 5-10%. The number of sampled dwellings below and above the reference level in each area are 107 and 31, 46 and 6, and 234 and 5 respectively, resulting in a percentage of houses in each EPA classification above the reference level of 2%, 12%, and 22% respectively.

4. Discussion

4.1. Soil-gas radon measurements

From the 48 soil-gas samples, 10 were taken above Tertiary granite, felsite formation; 3 above Tertiary basic intrusions; 15 above Silurian sandstone, greywacke, shale; 18 above Marine shelf facies; and 2 above Tertiary minor volcanics (Figure 1). The boxplot suggests there are some differences between formations (Figure 7), with the highest values in sub-soil above the Tertiary granite, felsite (granites) and Marine shelf facies (Carboniferous limestones) Formation, and the lowest values from subsoil above the Tertiary basic intrusion (dolerite & gabbro) and the Silurian sandstone, greywacke, shale (Silurian metasediments) Formation. The fact that houses built above the Silurian sandstone, greywacke, shale formation have the lowest indoor radon concentrations (Figure 8) confirms the importance of gaining a better understanding of the relationship between soil-gas radon concentration and indoor radon concentration.

Overall, 2-D analysis (Figure 4a) shows that the Cooley Peninsula is characterised by moderate soil-gas radon concentrations (30-50 kBq m^{-3}), without a clear correlation with geological units or fault systems (Figure 1). However, the lowest values are at the south-west and northern part of the Cooley Peninsula, related with the Silurian metasediments of the area. The highest soil-gas radon area is in the east part of the peninsula, related to the Carboniferous limestone. Finally, very high soil-gas radon values are found in the central granite area (igneous intrusion), two points in the N-W and one at S-E of this area, suggesting that the main fracture system (NW-SE direction) may influence radon concentration. Nevertheless, the lack of correlation between geology and soil-gas radon concentration may be the result of the relatively low sample density or the result of heterogeneity of the soil formations, and additional soil-gas sample sites would be needed to be targeted to further test such a correlation.

4.2. Radon potential classification

The radon potential map constructed based on active soil-gas radon measurements and soil permeability was compared with an existing radon hazard map based solely on seasonally adjusted indoor radon measurements. The Cooley Peninsula is mostly classified as High (H) and Moderate-High (M-H) radon potential (i.e. 84% of the total grids of 1 x 1 km; Figure 5) while in the Indoor Radon Map

for this area is classified as a High Radon Area (estimate percentage of houses above the reference level higher than 20%; Figure 6).

The very small number of houses tested for indoor radon concentration in areas classified as low risk (i.e. 5 dwellings) do not aid interpretation of results in these areas (Table 4), and the high probability obtained (20 %) does not seem realistic. These grids (i.e. 3 of 185; Figure 5) would therefore require further investigation in other to evaluate if the radon risk in this area is reality low, or if it should be classified as moderate. In the other radon risk areas however the geometric mean and the probability of having an indoor radon concentration above the reference level increases with the risk classification (Table 4). In this sense, the geometric mean increases from 34 Bq m^{-3} in M-L areas to 46 Bq m^{-3} in M-H, and 87 Bq m^{-3} in H areas, while the probability of having a high indoor radon concentration in M-L areas is about 4% (i.e. 5 dwelling of 140 have an indoor radon concentration higher than the reference level; Table 4), in M-H areas it is about 7% (i.e. 13 of 177), and in H areas it is 21% (23 of 107).

The probabilities of houses with radon concentrations above the reference level in the high radon potential areas (i.e. H-M and H) are in agreement with the EPA results, as calculated from indoor radon measurements, at around 12% for the 10-20% EPA band classification, and 22% for the >20% band (Figure 6). The false negatives for M-L radon potential areas (i.e. that the indoor radon concentrations are above the reference level when the area is classified as M-L radon potential area) are around 12% (5 of 42 dwellings; Table 4). On the other hand, the false positives (i.e. that the indoor radon concentrations are below the reference level when the area is classified as M-H or H radon potential area) are 42% (164 of 378) and 22% (84 of 387) respectively. These errors seem reasonable taking into account the uncertainties and spatial variability of indoor radon concentrations, and are in agreement with the EPA classification based on indoor radon measurements alone (i.e. false negative: 12%; false positive: 40%).

4.3. Indoor radon measurements

From the six 10x10 km grids sampled in the Cooley Peninsula, the EPA classified five as High Radon Areas (Figure 6). However, indoor radon measurements were clustered around populated and coastal areas of the Cooley Peninsula. Therefore, classification of the grids (10x10 km) was carried out without data in certain areas (e.g. centre area of the peninsula), and some misinterpretation of radon hazard could result. An ANOVA analysis (Table 5) showed that bedrock geology explains about 21% of the indoor radon variation (p-value < 0.01), with the Silurian Sandstone, Greywacke and Shale Formation

(Silurian metasediments) being the formation which statistically differed from the others, with a lower indoor radon concentrations (Figure 8a).

These results show that the proportion of indoor radon variation explained by bedrock geology is similar, for example, to the values obtained in England and Wales (i.g. 25%; Appleton and Miles, 2010), and Scotland (i.e. 21%; Scheib et al., 2009), and lightly higher than the variance explained in Northern Ireland (i.e. around 12-14%; Appleton et al., 2015) and SW England (i.e. about 10%; Ferreira et al., 2016). It is noteworthy that these areas have similar building standards and climate conditions. However, despite the small differences in the variance explained by bedrock geology, its influence on indoor radon concentration is significant in all cases and should be taken into account in radon risk assessment.

Comparing soil-gas and indoor radon concentrations, ANOVA analysis indicates that approximately 12% of the variance of indoor radon concentration can be explained by the predictions of soil-gas radon concentrations (p-value < 0.01). If soil permeability and geology are also taken into account, the model can explain up to 30% of indoor radon variance; 12% soil-gas radon predictions, 9.3% permeability and 8.6% geology (32% if the interaction between soil-gas radon and geology is added; the only interaction which is statistically significant, p-value < 0.01). These results confirm that soil-gas radon concentration is the main factor controlling the indoor radon concentration, but soil permeability and geology also have an important contribution. If each dataset is analysed separately, the explained variance is 12%, 18% and 21% for predicted soil-gas radon concentration, permeability and geology; respectively. The reduction of the percentage of variance explained by permeability and geology suggest that part of the information given by these datasets are already included in the soil-gas radon concentration predictions.

A logistic regression analysis (see Elío et al., 2017 for a full explanation of the methodology) confirms that with respect to indoor radon, the Silurian sandstone, greywacke, shale Formation is the only statistically different formation for the study area. Furthermore, the odds of having an indoor radon concentration above the reference level increases by a factor of 0.12 with respect to the Tertiary granite felsite. The predicted probabilities of exceeding the reference level are 19% for the Tertiary granite felsite; 18% for Tertiary basic intrusion, 3% for Silurian sandstone, greywacke, shale; 24% for Marine shelf facies, and 33% for Tertiary minor volcanics (Figure 8b). In agreement with the probability estimated assuming a log-normal distribution of the data (Table 6), the small differences can be related to the small number of data in some formations.

411

412 **4.4. Implications for indoor radon mapping**

413

414 Different options for mapping indoor radon risk were compared with the indoor radon measurements
415 (n = 429) by logistic regression (Table 7). The selection of the model was carried out in accordance
416 with the Akaike Information Criterion or AIC (being AIC = −2 log(Lik) + 2p, where Lik is the verisimilitude
417 of the model, and p the number of parameters of the model; Akaike, 1974). If the difference between
418 AIC in two models is greater than 2, the model with the lesser AIC is chosen but if the difference is
419 between 1 and 2, the models could be considered as being intimately linked (Anderson and Burnham
420 1999).

421

422 The classification based on indoor radon measurements (both the EPA classification - Figure 6-, which
423 divides the area in grids of 10x10 km, and InRn_BED500 classification - Figure 8b-, which divides the
424 area by different geological formations) has the lowest AIC (Table 7). This means that both these
425 models better explain the results of indoor radon concentrations. The AIC difference between these
426 two models was between 1 and 2, thus it could be considered that they give the same information.
427 However, it seems more appropriate to divide the area by geological units, and not by grids, since
428 geology is the main factor that controls the indoor radon concentrations (up to 21% in the Cooley
429 Peninsula, and around 10-25% in other countries with similar building standards). In this case, the false
430 positive error is increased slightly (from 12% to 19%), but it is probable that this error can be reduced
431 with a random stratified sampling design. The false positive value, however, is reduced from 40% to
432 29%.

433

434 Although radon potential (RP) maps only take into account the radon concentration in the soil-gas and
435 the soil permeability, the radon risk classification (i.e. Low, Moderate-Low, Moderate-High, High risk;
436 Figure 7) may be acceptable since the amount of data and the time required for the site classification
437 is substantially lower than that required for standard indoor radon measurements. In this regard, only
438 60 radon soil-gas samples (and 1 week) were required for site classification in this study, while more
439 than 400 indoor radon measurements (and 3 months for sampling indoor radon concentration) were
440 necessary for the EPA classification. Furthermore, if more detail were required, a follow-up field
441 campaign could be implemented in order to increase the number of soil-gas and soil permeability
442 measurements, rather than relying solely on indoor radon measurements.

443

In this regard soil-gas radon monitoring campaigns are viewed as cost effective when conducted at a local scale. Given that such an approach for radon potential classification only depends on geological factors and not on the type of dwellings or living styles (e.g. installation of radon barriers in the house, type of building, ventilation), it helps to minimise the temporal or spatial variability associated with indoor radon measurements. Furthermore, indoor radon measurements can potentially result in inaccurate risk evaluation in non-sampled areas, however, no such impediment affects soil-gas surveys where a grid-like sampling strategy is employed.

The disadvantage of in-situ soil measurements is that their applicability is locally limited due to physical restrictions. On a local scale, the density of in-situ measurements could be incremented to better estimate radon concentration and permeability in the soil (e.g. using geostatical methods), and in extreme cases the site for each new building could be characterised prior to its construction (e.g. the legal procedure in the Czech Republic; Neznal et al., 2010). However, at a national or regional scale it may be not possible to carry out a survey of in-situ radon soil-gas measurements with the required resolution within a short time-frame. The application of radon potential classification may therefore require evaluation of other cost-effective detection techniques, such airborne radiometric surveys, capable of covering large areas (e.g. Appleton et al., 2008; Appleton et al., 2011b).

In this study soil-gas radon measurements were carried out at 75-100 cm depth. We assumed therefore a minimal influence from external atmospheric factors such as temperature and pressure (García-González et al. 2008; Buttafuoco et al. 2010; Michel-le pierres et al. 2010; De Miguel et al. 2018), and that short-term variation in radon concentration occurs mainly at shallower depths in the soil profile (Schubert and Schulz 2002; Papp et al. 2014). This measuring depth is a standard procedure for evaluating the radon potential (Kemski et al. 2001; Neznal et al. 2004; Barnet 2012; Cosma et al. 2013; Szabó et al. 2014; Cinelli et al. 2015; Pásztor et al. 2016). However, some authors have suggested that atmospheric parameters may still have an influence over a short time-scale even at a depth greater than 80 cm (Zmazek et al. 2002; Cigolini et al. 2009). We have used a control point to verify that there were no significant variations between the 5 days of the fieldwork, and the data collected are therefore suitable for the purpose of our study.

Continuous monitoring may however help to better understand the role of atmospheric factors (e.g. pressure, temperature, soil humidity), and other gas phases (e.g. CO_2), on the ^{222}Rn levels in soil. High seasonal/daily variations on soil-gas radon concentration may generate uncertainties in the risk assessment (i.e. Radon Potential; RP), and RP may therefore require a seasonal adjustment (Szabó et

al. 2013). However, since there is not a general dependence of atmospheric factors on soil gas radon concentration (Szabó et al. 2013), and different patterns may occur under similar climate conditions depending on the soil type (King and Minissale 1994), specific long-term campaigns would be needed in order to define national/regional seasonal correction factors.

Soil permeability has a high influence in indoor radon, and better estimation of this parameter will increase the quality of results. The efforts to characterise a site should be focused, therefore, not only on radon measurements but also on direct measurement of gas permeability of the soil. Although hydraulic conductivity or subsoil permeability estimations are normally available on a national scale (or other datasets, e.g. soil type), it is highly recommended to carry out in-situ gas permeability measurements at the same sites as soil-gas monitoring in order to validate the permeability classification in relation to radon protection.

Finally, if the measurement of indoor radon concentration were the preferred strategy selected for radon mapping, it could be more accurate to divide the sampled area according to geological units, not by grids, since geology is the main factor controlling indoor radon concentration. At a national scale, a varied approach could be employed using a combination of dividing a country into grids and then, dividing each grid into geological units. In this way, other factors that may be as important as geology (e.g. atmospheric conditions, building characteristics, altitude, etc.) can be homogenized in the grid, with the geology subsequently taken into account. Where possible, a random sampling of dwellings overlying each geological unit could avoid the clustering of indoor radon measurements, and although the unpopulated areas will be still not be sampled, geological factors may help to more accurately interpret the radon risk.

5. Conclusions

A method to carry out a radon potential classification using 60 in-situ radon measurements in 48 sites was tested and validated in a case study of an area of approximately 160 km^2 in the Cooley Peninsula, NE Ireland. Although the number of samples sites is relatively low, the results obtained show that the radon potential map is generally in agreement with the results of the Indoor Radon Map, and thus rapid local soil-gas surveys can be helpful as a cost-effective means to complement radon risk maps based on indoor radon measurements, or produce a radon potential map where no prior indoor radon measurements have taken place.

The percentage of indoor radon variance explained by soil-gas radon concentration, subsoil permeability and geology was approximately 30% (12%, 9.3% and 8.6%, respectively). This result confirms that although soil-gas radon concentration is the parameter which explains the greatest degree of variance, subsoil permeability and geology also have a high influence and should be taken into account for evaluating radon risk.

Acknowledgements

Many thanks to Louth County Council and Alec Rolston (Dundalk Institute of Technology) for their help during the sampling design. Luka Vucinic (Trinity College Dublin) and Aileen Doran (Geological Survey, Ireland) are gratefully acknowledged for assistance in the field.

This work has been financed by the Irish Research Council (IRC - Enterprise Partnership Scheme Postdoctoral Fellowship 2015; Enterprise Partner: Geological Survey, Ireland; EPSPD/2015/46), and co-financed by the Geological Survey, Ireland (GSI research programme Short Call 2017; Ref. Number: 2017-SC-008). The sole responsibility of this publication lies with the authors. The GSI and IRC are not responsible for any use that may be made of the information contained therein. The Environmental Protection Agency of Ireland have also partly financed the present study purchasing the required instrumentation. Data used in this project were collated as part of the Tellus projects (www.tellus.ie), and also by the Environmental Protection Agency of Ireland and the Geological Survey, Ireland.

References

Adepelumi AA, Ajayi TR, Ako BD, Ojo AO (2005) Radon soil-gas as a geological mapping tool: case study from basement complex of Nigeria. Environ Geol 48:762–770. doi: 10.1007/s00254-005-0016-0

Akaike H (1974) A new look at the statistical model identification. IEEE Trans Automat Contr 19:716–723. doi: 10.1109/TAC.1974.1100705

Andersen CE (2001) Numerical modelling of radon-222 entry into houses: An outline of techniques and results. Sci Total Environ 272:33–42. doi: 10.1016/S0048-9697(01)00662-3

Anderson DR, Burnham KP (1999) Understanding information criteria for selection among capture-recapture or ring recovery models. Bird Study 46:S14–S21. doi: 10.1080/00063659909477227

Appleton JD, Cave MR, Miles JCH, Sumerling TJ (2011a) Soil radium, soil gas radon and indoor radon empirical relationships to assist in post-closure impact assessment related to near-surface radioactive waste disposal. J Environ Radioact 102:221–234. doi:

10.1016/j.jenvrad.2010.09.007
Appleton JD, Daraktchieva Z, Young ME (2015) Geological controls on radon potential in Northern Ireland. Proc Geol Assoc 126:328–345. doi: 10.1016/j.pgeola.2014.07.001
Appleton JD, Doyle E, Fenton D, Organo C (2011b) Radon potential mapping of the Tralee–Castleisland and Cavan areas (Ireland) based on airborne gamma-ray spectrometry and geology. J Radiol Prot 31:221–235. doi: 10.1088/0952-4746/31/2/002
Appleton JD, Miles JCH (2010) A statistical evaluation of the geogenic controls on indoor radon concentrations and radon risk. J Environ Radioact 101:799–803. doi: 10.1016/j.jenvrad.2009.06.002
Appleton JD, Miles JCH, Green BMR, Larmour R (2008) Pilot study of the application of Tellus airborne radiometric and soil geochemical data for radon mapping. J Environ Radioact 99:1687–97. doi: 10.1016/j.jenvrad.2008.03.011
Appleton JD, Miles JCH, Young M (2011c) Comparison of Northern Ireland radon maps based on indoor radon measurements and geology with maps derived by predictive modelling of airborne radiometric and ground permeability data. Sci Total Environ 409:1572–83. doi: 10.1016/j.scitotenv.2011.01.023
Azam A, Naqvi AH, Srivastava DS (1995) Radium concentration and radon exhalation measurements using LR-115 type II plastic track detectors. Nucl. Geophys. 9:653–657
Barnet I (2012) Indoor radon probability calculated from the Czech soil gas radon data in a grid net for the European Geogenic Radon Map construction: test of feasibility. Environ Earth Sci 66:1149–1153. doi: 10.1007/s12665-011-1322-3
Baxter S (2008) A Geological Field Guide to Cooley, Gullion, Mourne & Slieve Croob
Baykut S, Akgül T, Inan S, Seyis C (2010) Observation and removal of daily quasi-periodic components in soil radon data. Radiat Meas 45:872–879. doi: 10.1016/j.radmeas.2010.04.002
Bivand RS, Pebesma EJ, Gómez-Rubio V (2008) Applied Spatial Data Analysis with R. Springer New York, New York, NY
Bonotto DM, Andrews JN (1999) Transfer of radon and parent nuclides 238U and 234U from soils of the Mendip Hills area, England, to the water phase. J Geochemical Explor 66:255–268. doi: 10.1016/S0375-6742(99)00016-3
Bossew P (2015) Mapping the Geogenic Radon Potential and Estimation of Radon Prone Areas in Germany. Radiat Emerg Med 4:13–20
Bossew P, Tollefsen T, Cinelli G, et al (2015) Status of the European Atlas of Natural Radiation. Radiat Prot Dosimetry 167:29–36. doi: 10.1093/rpd/ncv216
BSI (1999) Code of practice for site investigations. BS 5930:1999. Br Stand

581 Burke Ó, Long S, Murphy P, et al (2010) Estimation of seasonal correction factors through Fourier
582 decomposition analysis—a new model for indoor radon levels in Irish homes. J Radiol Prot
583 30:433–443. doi: 10.1088/0952-4746/30/3/002
584 Buttafuoco G, Tallarico A, Falcone G, Guagliardi I (2010) A geostatistical approach for mapping and
585 uncertainty assessment of geogenic radon gas in soil in an area of southern Italy. Environ Earth
586 Sci 61:491–505. doi: 10.1007/s12665-009-0360-6
587 Capaccioni B, Cinelli G, Mostacci D, Tositti L (2012) Long-term risk in a recently active volcanic
588 system: Evaluation of doses and indoor radiological risk in the quaternary Vulsini Volcanic
589 District (Central Italy). J Volcanol Geotherm Res 247–248:26–36. doi:
590 10.1016/j.jvolgeores.2012.07.014
591 Chen J, Rahman NM, Abu Atiya I (2010) Radon exhalation from building materials for decorative use.
592 J Environ Radioact 101:317–22. doi: 10.1016/j.jenvrad.2010.01.005
593 Cigolini C, Poggi P, Ripepe M, et al (2009) Radon surveys and real-time monitoring at Stromboli
594 volcano: Influence of soil temperature, atmospheric pressure and tidal forces on222Rn
595 degassing. J Volcanol Geotherm Res 184:381–388. doi: 10.1016/j.jvolgeores.2009.04.019
596 Cinelli G, Tositti L, Capaccioni B, et al (2015) Soil gas radon assessment and development of a radon
597 risk map in Bolsena, Central Italy. Environ Geochem Health 37:305–319. doi: 10.1007/s10653-
598 014-9649-9
599 Colgan P, Organo C, Hone C, Fenton D (2008) Radiation doses received by the Irish population
600 Cosma C, Cucoş-Dinu A, Papp B, et al (2013) Soil and building material as main sources of indoor
601 radon in Bâiţa-ştei radon prone area (Romania). J Environ Radioact 116:174–179. doi:
602 10.1016/j.jenvrad.2012.09.006
603 Cothern R (1999) Indoor air radon. Environ Geochem Health 21:83–90. doi:
604 10.1023/A:1006655431280
605 Cothern R, Smith J (1987) Environmental radon. Plenum Press, New York
606 De Miguel E, Barrio-Parra F, Elío J, et al (2018) Applicability of radon emanometry in lithologically
607 discontinuous sites contaminated by organic chemicals. Environ Sci Pollut Res 25:20255–20263.
608 doi: 10.1007/s11356-018-2372-9
609 Dowdall A, Murphy P, Pollard D, Fenton D (2017) Update of Ireland's national average indoor radon
610 concentration – Application of a new survey protocol. J Environ Radioact 169:1–8. doi:
611 10.1016/j.jenvrad.2016.11.034
612 Dubois G (2005) An Overview of Radon Surveys in Europe (EUR 21892 EN). Office for Official
613 Publication of the European Communities, Luxembourg
614 Elío J, Crowley Q, Scanlon R, et al (2018) Estimation of residential radon exposure and definition of

615 Radon Priority Areas based on expected lung cancer incidence. Environ Int 114:69–76. doi:
616 10.1016/j.envint.2018.02.025
617 Elío J, Crowley Q, Scanlon R, et al (2017) Logistic regression model for detecting radon prone areas in
618 Ireland. Sci Total Environ 599–600:1317–1329. doi: 10.1016/j.scitotenv.2017.05.071
619 Elío J, Ortega MF, Nisi B, et al (2015a) CO2 and Rn degassing from the natural analog of Campo de
620 Calatrava (Spain): Implications for monitoring of CO2 storage sites. Int J Greenh Gas Control
621 32:1–14. doi: 10.1016/j.ijggc.2014.10.014
622 Elío J, Ortega MF, Nisi B, et al (2015b) Evaluation of the applicability of four different radon
623 measurement techniques for monitoring CO<inf>2</inf> storage sites. Int J Greenh Gas Control
624 41:. doi: 10.1016/j.ijggc.2015.06.021
625 Etiope G, Martinelli G (2002) Migration of carrier and trace gases in the geosphere: an overview.
626 Phys Earth Planet Inter 129:185–204. doi: 10.1016/S0031-9201(01)00292-8
627 EURATOM (2013) Council Directive 2013/59/EURATOM of 5 December
628 Fennell SG, Mackin GM, Madden JS, et al (2002) Radon in Dwellings The Irish National Radon Survey
629 (Report RPII-02/1). Radiological Protection Institute of Ireland
630 Ferreira A, Daraktchieva Z, Beamish D, et al (2018) Indoor radon measurements in south west
631 England explained by topsoil and stream sediment geochemistry, airborne gamma-ray
632 spectroscopy and geology. J Environ Radioact 181:152–171. doi: 10.1016/j.jenvrad.2016.05.007
633 Field RW (2015) Radon: An Overview of Health Effects. In: Reference Module in Earth Systems and
634 Environmental Sciences. Elsevier
635 Gallagher V, Knights K, Carey S, et al (2016) Atlas of Topsoil Geochemistry of the Northern Counties
636 of Ireland. Data from the Tellus and Tellus Border Projects
637 García-González JE, Ortega MF, Chacón E, et al (2008) Field validation of radon monitoring as a
638 screening methodology for NAPL-contaminated sites. Appl Geochemistry 23:2753–2758. doi:
639 10.1016/j.apgeochem.2008.06.020
640 Giammanco S, Immè G, Mangano G, et al (2009) Comparison between different methodologies for
641 detecting radon in soil along an active fault: The case of the Pernicana fault system, Mt. Etna
642 (Italy). Appl Radiat Isot 67:178–185. doi: 10.1016/j.apradiso.2008.09.007
643 Giammanco S, Sims KWW, Neri M (2007) Measurements of 220 Rn and 222 Rn and CO 2 emissions in
644 soil and fumarole gases on Mt. Etna volcano (Italy): Implications for gas transport and shallow
645 ground fracture. Geochemistry, Geophys Geosystems 8:n/a-n/a. doi: 10.1029/2007GC001644
646 Greeman DJ, Rose AW (1996) Factors controlling the emanation of radon and thoron in soils of the
647 eastern U.S.A. Chem Geol 129:1–14. doi: 10.1016/0009-2541(95)00128-X
648 Groves-Kirkby CJ, Crockett RGM, Denman AR, Phillips PS (2015) A critical analysis of climatic

649 influences on indoor radon concentrations: Implications for seasonal correction. J Environ
650 Radioact 148:16–26. doi: 10.1016/j.jenvrad.2015.05.027
651 Guerra M, Etiope G (1999) Effects of gas-water partitioning, stripping and channelling processes on
652 radon and helium gas distribution in fault areas. Geochem J 33:141–151
653 Gunby JA, Darby SC, Miles JCH, et al (1993) Factors Affecting Indoor Radon Concentrations in the
654 United Kingdom. Health Phys 64:2–12. doi: 10.1097/00004032-199301000-00001
655 Gunning GA, Pollard D, Finch EC (2014) An outdoor radon survey and minimizing the uncertainties in
656 low level measurements using CR-39 detectors. J Radiol Prot 34:457–467. doi: 10.1088/0952-
657 4746/34/2/457
658 Hodgson J, Carey S (2013) Tellus Border project: Radon risk predictive modelling using airborne
659 geophysical data in the border region of Ireland
660 Hodgson J, Carey S, Scanlon R (2014) Developing a new National Radon Risk Map. Dublin, Ireland
661 HSE (2013) Pattern of radon levels - Ireland Data source : RPII. Ireland
662 Hunter Williams NH, Misstear BDR, Daly D, Lee M (2013) Development of a national groundwater
663 recharge map for the Republic of Ireland. Q J Eng Geol Hydrogeol 46:493–506. doi:
664 10.1144/qjegh2012-016
665 Huxol S, Brennwald MS, Hoehn E, Kipfer R (2012) On the fate of 220Rn in soil material in dependence
666 of water content: Implications from field and laboratory experiments. Chem Geol 298–
667 299:116–122. doi: 10.1016/j.chemgeo.2012.01.002
668 Kemski J, Siehl A, Stegemann R, Valdivia-Manchego M (2001) Mapping the geogenic radon potential
669 in Germany. Sci Total Environ 272:217–230. doi: 10.1016/S0048-9697(01)00696-9
670 King CY, Minissale A (1994) Seasonal variability of soil-gas radon concentration in central California.
671 Radiat Meas 23:683–692. doi: 10.1016/1350-4487(94)90004-3
672 Lee M, Hunter-Williams N, Meehan R, et al (2008) Groundwater vulnerability mapping. In: Irish
673 National Hydrology Conference. Tullamore, Ireland
674 Long S, Fenton D, Cremin M, Morgan a (2013) The effectiveness of radon preventive and remedial
675 measures in Irish homes. J Radiol Prot 33:141–9. doi: 10.1088/0952-4746/33/1/141
676 Masterson S, Kelly C, Lee M (2008) County Cavan Groundwater Protection Scheme Volume I : Main
677 Report Final
678 McColl N, Auvinen A, Kesminiene A, et al (2015) European Code against Cancer 4th Edition: Ionising
679 and non-ionising radiation and cancer. Cancer Epidemiol 39 Suppl 1:S93-100. doi:
680 10.1016/j.canep.2015.03.016
681 Michel-le pierres K, Gal F, Brach M, Guignat S (2010) Radon, helium and CO2 measurements in soils
682 overlying a former exploited oilfield, Pechelbronn district, Bas-Rhin, France. J Environ Radioact

683 101:835–846. doi: 10.1016/j.jenvrad.2010.05.006
684 Neznal M, Neznal M, Barnet I (2010) Practical usefulness of radon risk maps and detailed in-situ
685 classification of radon risk. Nukleonika 55:471–475
686 Neznal M, Neznal M, Matolín M, et al (2004) New Method for Assessing the Radon Risk of Building
687 Sites. Czech Geol Surv Spec Pap
688 NRCS (2014) National Radon Control Strategy, Minister for the Environment (Ireland)
689 Oufni L, Manaut N, Taj S, Manaut B (2013) Determination of Radon and Thoron Concentrations in
690 Different Parts of Some Plants Used in Traditional Medicine Using Nuclear Track Detectors. Am
691 J Environ Prot 1:34–40. doi: 10.12691/env-1-2-4
692 Papp B, Szakács A, Néda T, et al (2014) Soil radon and thoron activity concentrations and CO2 flux
693 measurements in the neogene volcanic region of the Eastern Carpathians (Romania).
694 Carpathian J Earth Environ Sci 9:261–268
695 Pásztor L, Szabó KZ, Szatmári G, et al (2016) Mapping geogenic radon potential by regression kriging.
696 Sci Total Environ 544:883–891. doi: 10.1016/j.scitotenv.2015.11.175
697 Porcelli D (2008) Chapter 4 Investigating Groundwater Processes Using U- and Th-Series Nuclides.
698 Radioact Environ 13:105–153. doi: 10.1016/S1569-4860(07)00004-6
699 Prasad G, Ishikawa T, Hosoda M, et al (2012) Estimation of radon diffusion coefficients in soil using
700 an updated experimental system. Rev Sci Instrum 83:. doi: 10.1063/1.4752221
701 Sarra A, Fontanella L, Valentini P, Palermi S (2016) Quantile regression and Bayesian cluster
702 detection to identify radon prone areas. J Environ Radioact 164:354–364. doi:
703 10.1016/j.jenvrad.2016.06.014
704 Scheib C, Appleton J, Miles J, Hodgkinson E (2013) Geological controls on radon potential in England.
705 Proc Geol Assoc 124:910–928. doi: 10.1016/j.pgeola.2013.03.004
706 Scheib C, Appleton JD, Miles JCH, et al (2009) Geological controls on radon potential in Scotland.
707 Scottish J Geol 45:147–160. doi: 10.1144/0036-9276/01-401
708 Schubert M, Freyer K, Treutler HC, Weiß H (2001) Using the soil gas radon as an indicator for ground
709 contamination by non-aqueous phase-liquids. J Soils Sediments 1:217–222. doi:
710 10.1007/BF02987728
711 Schubert M, Peña P, Balcázar M, et al (2005) Determination of radon distribution patterns in the
712 upper soil as a tool for the localization of subsurface NAPL contamination. Radiat Meas 40:633–
713 637. doi: 10.1016/j.radmeas.2005.04.020
714 Schubert M, Schulz H (2002) Diurnal radon variations in the upper soil layers and at the soil-air
715 interface related to meteorological parameters. Health Phys 83:91–96. doi: 10.1097/00004032-
716 200207000-00010

717 Szabó KZ, Jordan G, Horváth Á, Szabó C (2014) Mapping the geogenic radon potential: methodology
718 and spatial analysis for central Hungary. J Environ Radioact 129:107–120. doi:
719 10.1016/j.jenvrad.2013.12.009
720 Szabó KZ, Jordan G, Horváth Á, Szabó C (2013) Dynamics of soil gas radon concentration in a highly
721 permeable soil based on a long-term high temporal resolution observation series. J Environ
722 Radioact 124:74–83. doi: 10.1016/j.jenvrad.2013.04.004
723 Tanner AB (1978) Radon migration in the ground: A supplementary review. Third Int Symp Nat
724 Radiat Environ 63
725 Tollefsen T, Cinelli G, Bossew P, et al (2014) From the European indoor radon map towards an atlas
726 of natural radiation. Radiat Prot Dosimetry 162:129–134. doi: 10.1093/rpd/ncu244
727 UNSCEAR (2000) Report of the united nations scientific committee on the effects of atomic radiation
728 to the general assembly. Sources Eff Ioniz Radiat
729 UNSCEAR (2006) Report to the General Assembly, with Scientific Annexes. Eff Ioniz Radiat
730 US-EPA (2003) EPA Assessment of Risks from Radon in Homes. Washington, DC
731 US-EPA (2001) Building Radon Out. A Step-by-Step Guide On How To Build Radon-Resistant Homes
732 WHO (2009) WHO Handbook on Indoor Radon: A Public Health Perspective. World Health
733 Organization, France
734 Zmazek B, Živčí M, Vaupotič J, et al (2002) Soil radon monitoring in the Krško Basin, Slovenia. Appl
735 Radiat Isot 56:649–657. doi: 10.1016/S0969-8043(01)00255-X
736

737 **Figure Captions:**

738

739 Figure 1: Radon soil-gas measurements in the Cooley Peninsula (Bedrock geology scale 1:500k;
740 download from Geological Survey Ireland, www.gsi.ie)

741

742 Figure 2: Radon potential classification

743

744 Figure 3: a) Optimal Box-Cox transformation of soil-gas radon measurements (lambda = 0.50), b)
745 normal q-q plot, c) histogram and d) experimental variogram of radon transformed data

746

747 Figure 4: a) Soil-gas radon (^{222}Rn) measurements and radon classification based on radon predictions
748 (inverse distance weighted interpolation; idp = 2, nmax = 10, grids 100x100m), and b) soil
749 permeability (GSI Groundwater Recharge Map)

750

751 Figure 5: Radon potential map at 1km grid squares. Indoor radon measurements are shown by green
752 dots (InRn < 200 Bq m^{-3}) and red stars (InRn > 200 Bq m^{-3})

753

754 Figure 6: Indoor Radon Risk Map at 10 km grid squares (EPA; after Fennell et al., 2002)

755

756 Figure 7: Box-plot soil-gas radon measurements (normally transformed). Unit Label: 9 - Tertiary
757 granite, felsite; 11 - Tertiary basic intrusion; 49 - Silurian sandstone, greywacke, shale; 64 - Marine
758 shelf facies; 78 - Tertiary minor volcanics

759

760 Figure 8: a) Box-plot indoor radon measurements (lognormal transformation). Unit Label: 9 - Tertiary
761 granite, felsite; 11 - Tertiary basic intrusion; 49 - Silurian sandstone, greywacke, shale; 64 - Marine
762 shelf facies; 78 - Tertiary minor volcanics. b) Estimate percentage of houses above the reference
763 level based on bedrock units (scale 1:500k) and indoor radon concentrations. Green dots: InRn < 200
764 Bq m^{-3}; Red starts: InRn > 200 Bq m^{-3}

765

766

Table Captions:

Table 1: Assigned values for the radon potential (RP) estimation

Table 2: Results of soil-gas radon concentration

Table 3: Control point and replicas

Table 4: Number of dwellings above the reference level in each radon potential (RP) area

Table 5: ANOVA tables for indoor radon concentration

Table 6: Number of dwellings above the reference level in each Formation

Table 7: AIC Criterion values for each of the four logistic regressions models

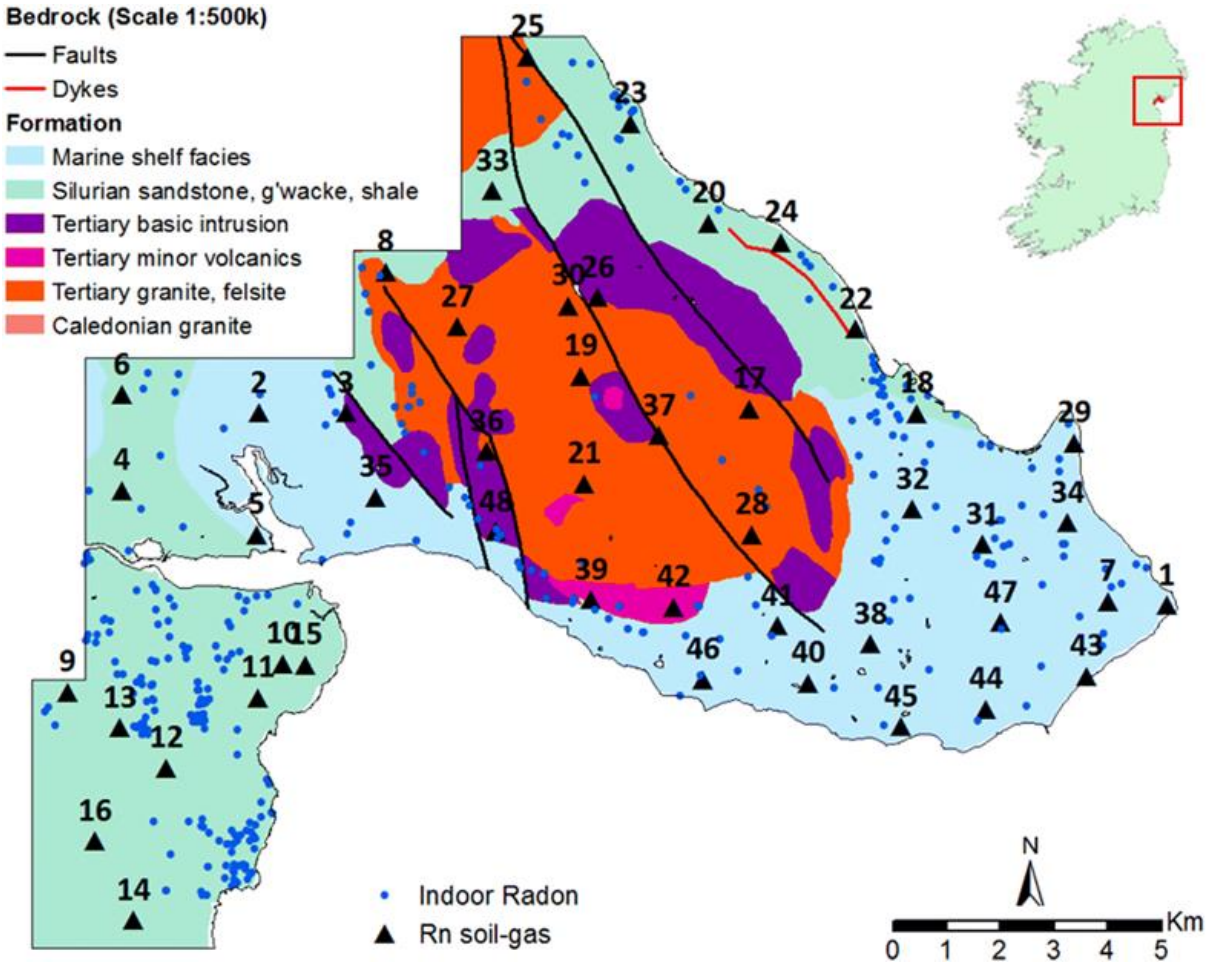

784

		Radon Potential (RP)					
Permeability	Low	2	8	17	22	28	37
	Moderate	3	13	25	33	43	55
	High	5	25	50	65	85	110
		Very Low	Low	Moderate	High	Very High	Extremely High
		Radon soil-gas classification					

785

786

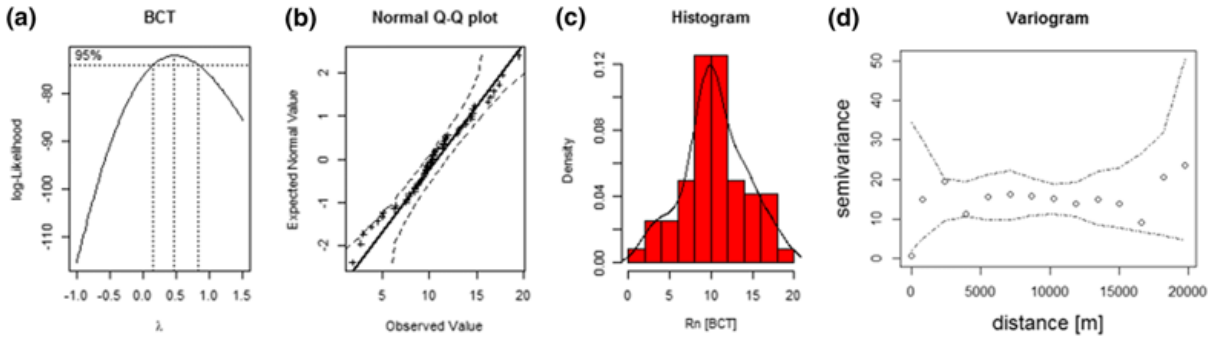

787

788

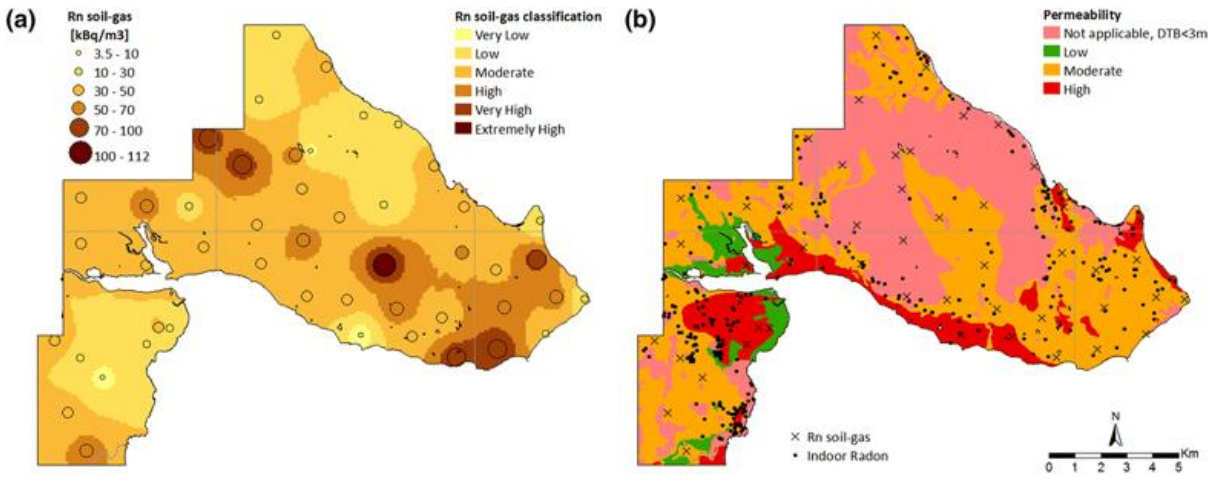

789

790

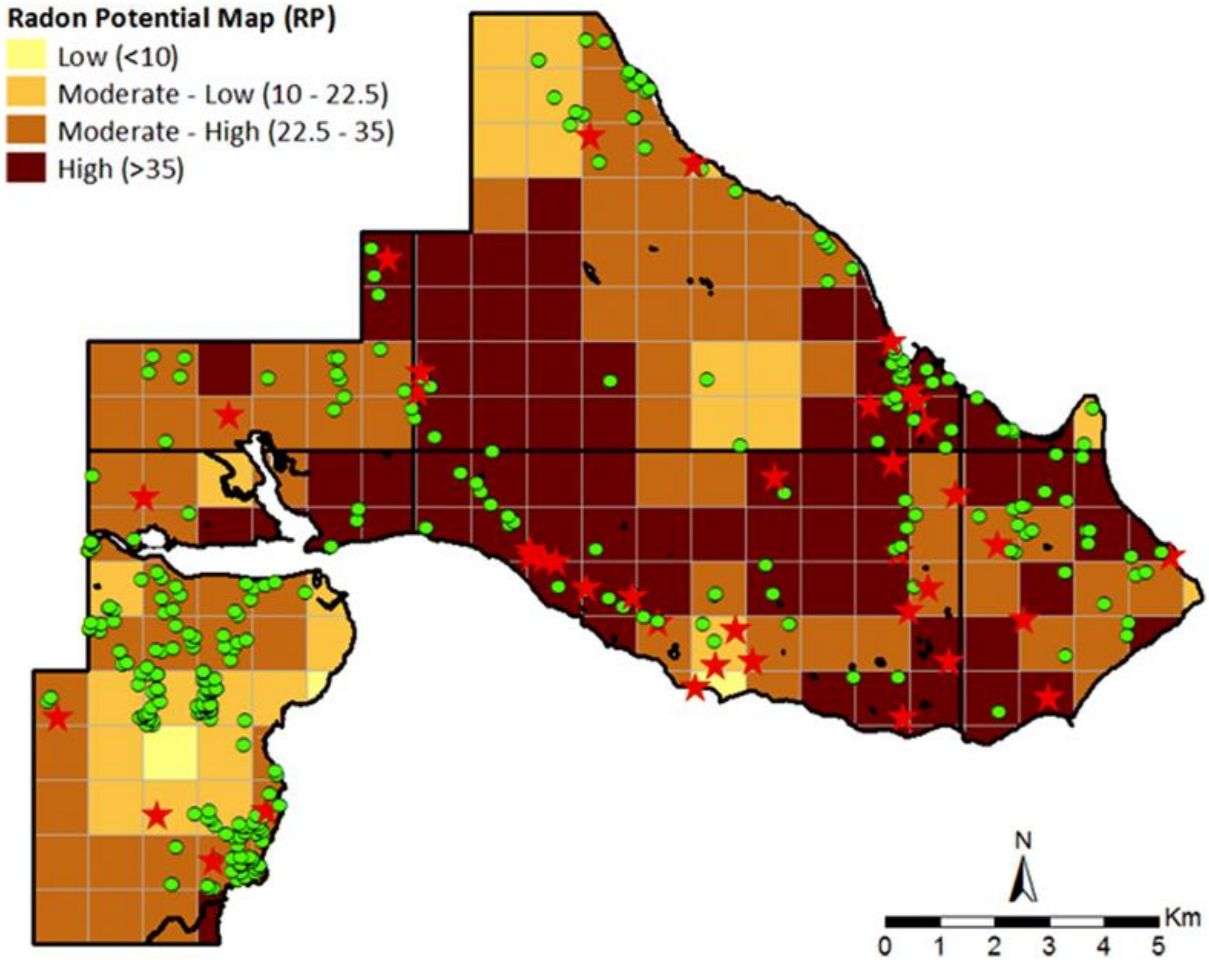
Radon Potential Map (RP)
Low (<10)
Moderate - Low (10 - 22.5)
Moderate - High (22.5 - 35)
High (>35)
N
Km
0 1 2 3 4 5

791

792

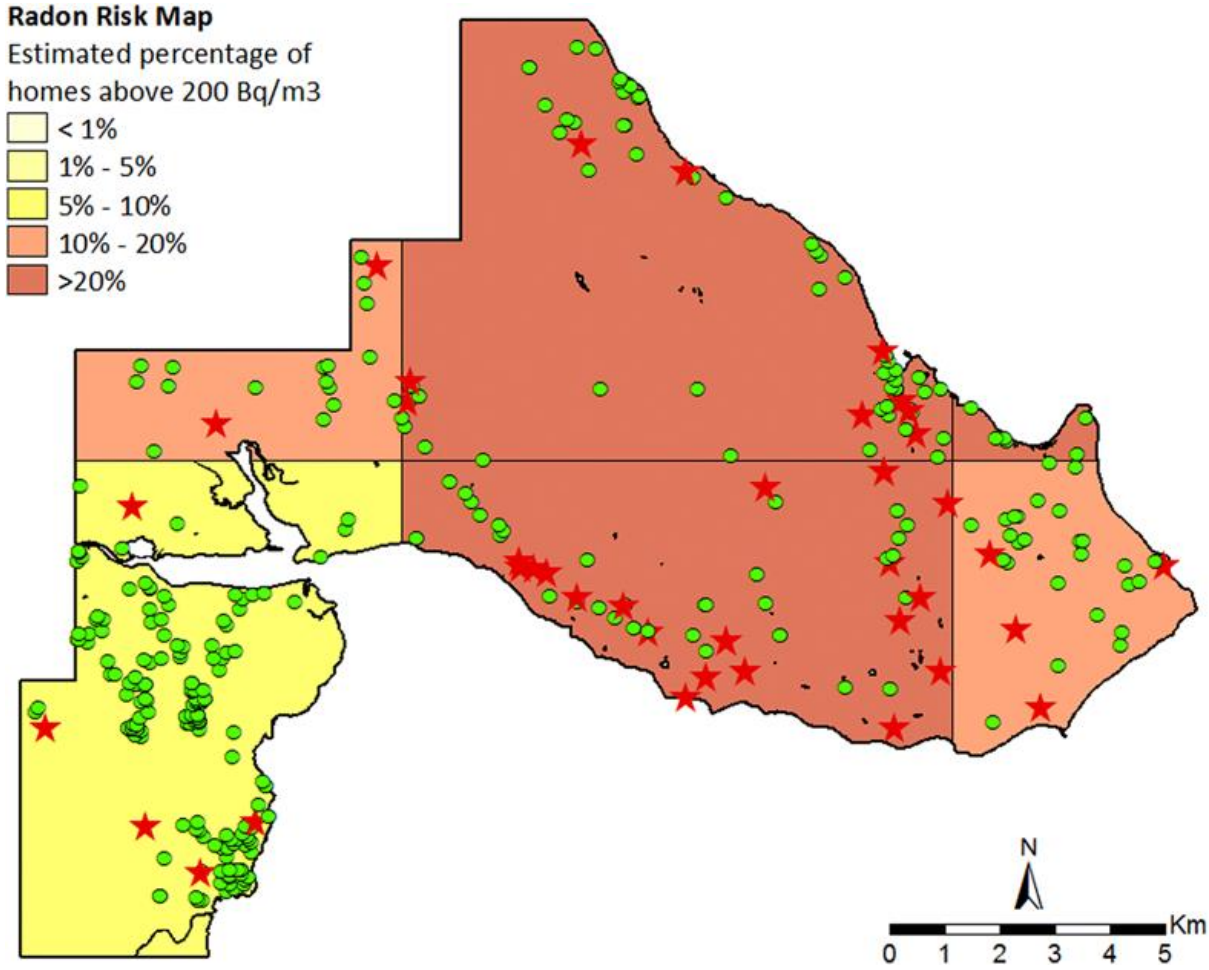
Radon Risk Map
Estimated percentage of
homes above 200 Bq/m3
< 1%
1% - 5%
5% - 10%
10% - 20%
>20%
N
Km
0 1 2 3 4 5

793

794

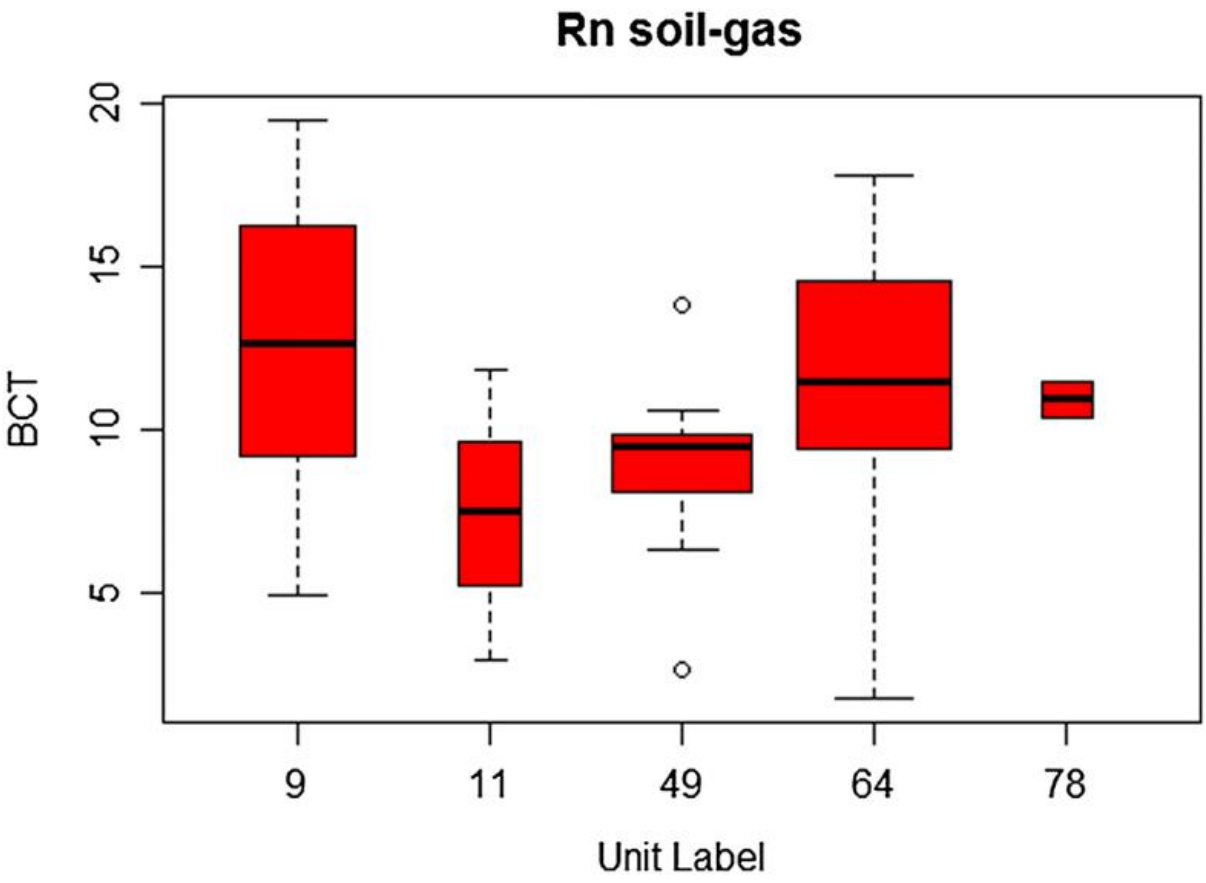
Rn soil-gas
BCT
20
15
10
5
9
11
49
64
78
Unit Label

795

796

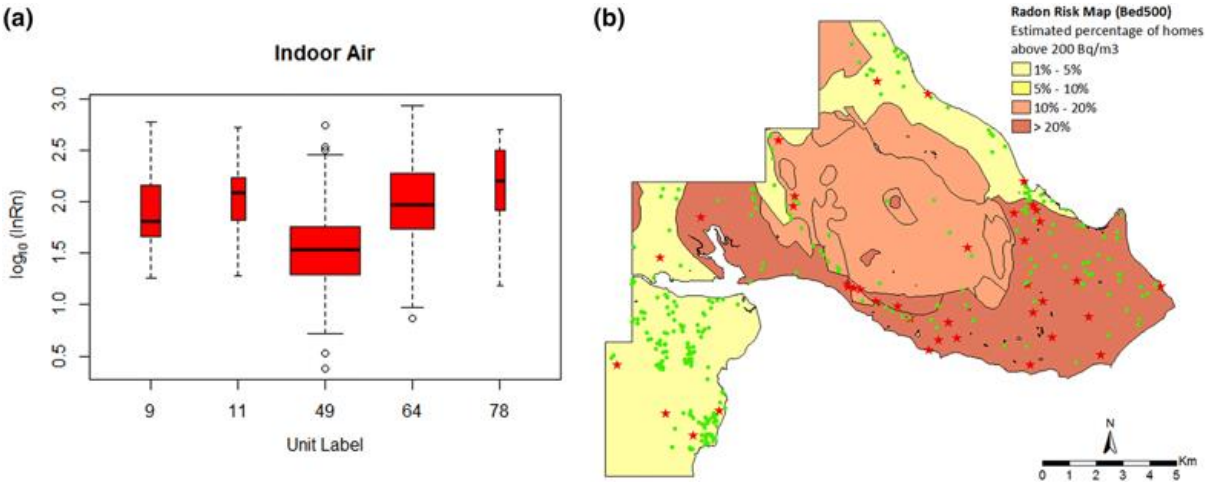
(a)
Indoor Air
log10 (lnRn)
3.0
2.5
2.0
1.5
1.0
0.5
9
11
49
64
78
Unit Label
(b)
Radon Risk Map (Bed500)
Estimated percentage of homes
above 200 Bq/m3
1% - 5%
5% - 10%
10% - 20%
> 20%
N
Km
0 1 2 3 4 5

797